Lecture Notes in Networks and Systems 696

Xin-She Yang
R. Simon Sherratt
Nilanjan Dey
Amit Joshi *Editors*

Proceedings of Eighth International Congress on Information and Communication Technology

ICICT 2023, London, Volume 4

Springer

Xin-She Yang · R. Simon Sherratt · Nilanjan Dey · Amit Joshi
Editors

Proceedings of Eighth International Congress on Information and Communication Technology

ICICT 2023, London, Volume 4

Springer

Editors
Xin-She Yang
Department of Design Engineering
and Mathematics
Middlesex University London
London, UK

Nilanjan Dey
Department of Computer Science
and Engineering
Techno International Newtown
Chakpachuria, West Bengal, India

R. Simon Sherratt
Department of Biomedical Engineering
University of Reading
England, UK

Amit Joshi
Global Knowledge Research Foundation
Ahmedabad, India

ISSN 2367-3370 ISSN 2367-3389 (electronic)
Lecture Notes in Networks and Systems
ISBN 978-981-99-3235-1 ISBN 978-981-99-3236-8 (eBook)
https://doi.org/10.1007/978-981-99-3236-8

A Two-Tape Design of Metamaterial Based on a Quasi-fractal Approach

Vadym Slyusar and Ihor Sliusar

Abstract Various options for the 3D design of a metamaterial cell based on two-ribbon split rings have been proposed and studied. When synthesizing the geometry of the outer tape, a quasi-fractal approach was used, which made it possible to form periodic sequences of depressions (slots) in its end surfaces. Their alternation from both ends of the tape was carried out synchronously or in a checkerboard pattern. In this case, the depth of all grooves could be fixed or changed according to a certain law. An Ansys HFSS electromagnetic simulator was used to study the properties of the proposed metamaterial cell designs. In the course of the research, the main attention was paid to determining the frequency ranges in which the dielectric permittivity and magnetic permeability take negative values (double-negative (DNG) zones). When a square conductor oriented perpendicular to the plane of the rings is included in the metacell, a relative bandwidth was achieved in the low-frequency zone, in which the condition of negative values of the dielectric permittivity and magnetic permeability is observed. The relative frequency band of the DNG zone in this case is 185.22%.

Keywords Ansoft HFSS · Quasi-fractal · Metamaterial · Refractive index · Relative permittivity and permeability · Split-ring resonator (SRR)

1 Introduction

The entry of humanity into the Internet of Things era has significantly expanded the range of tasks solved using wireless access technologies [1]. At the same time, taking into account the mobility of users of telecommunication services, preference

V. Slyusar (✉)
Central Research Institute of Armaments and Military Equipment of Armed Forces of Ukraine, Kyiv, Ukraine
e-mail: swadim@ukr.net

I. Sliusar
Poltava State Agrarian University, Poltava, Ukraine
e-mail: islyusar2007@ukr.net

X.-S. Yang et al. (eds.), *Proceedings of Eighth International Congress on Information and Communication Technology*, Lecture Notes in Networks and Systems 696,
https://doi.org/10.1007/978-981-99-3236-8_54

is given to compact solutions. Regardless of the frequency range used, the main ways to achieve miniaturization are, first of all, the use of electrically small antennas [2], as well as the use of metamaterials [3–8].

Since the elementary cells of a metamaterial in many cases have multi-component structures, the known set of approaches to the synthesis of such can be extended by passing to the 3D topology of their constituent elements [9–12].

2 The Aim of Research

The purpose of the report is to study the electromagnetic parameters of 3D SRR structures, in which the constituent elements are modeled on the basis of quasi-fractals.

3 The Main Results of the Study

The use of fractal solutions in radio engineering has been sufficiently tested and has proven itself on the positive side [13]. A similar approach can also be applied to the synthesis of metamaterial cells. In this work, the study of cells on a quasi-fractal basis was carried out in several stages. At the first of them, the object of analysis was two-ribbon split rings without a conductor, with end grooves in the outer tape. At the same time, the inner tape did not have such cutouts in its end surfaces. The grooves in the outer tape were obtained on the basis of the meander fractal initiator of the first iteration [1, 14]. The corresponding quasi-fractal technology used to synthesize the outer ring is based on the technique described in [15, 16]. The principle of groove formation is explained in detail in Fig. 1 [16].

It should be noted that double rings without a conductor make it possible to obtain zones of negative magnetic permeability that are broadband in frequency. This makes it possible to use them, for example, to form absorbers or magnetic metalenses.

The well-known Ansys HFSS simulator [17, 18] was used to study the electromagnetic properties of various options for the design of metamaterial cells. The 3D topology designer built into it made it possible to implement the configuration

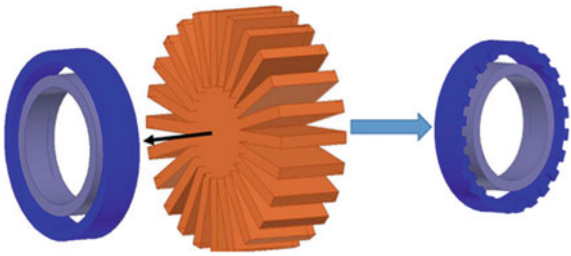

Fig. 1 Principle of formation of quasi-fractal grooves in the outer tape

shown in Fig. 1 method of forming end surfaces in the outer tape. The total number of grooves, similarly to [16], was set to 24, and they were located with a uniform step around the circumference with an angular interval of 15°.

To ensure the possibility of comparison with the previously obtained results, the geometric parameters of the metacell ribbon were set as follows: the thickness of the ribbons was 3 mm, the width was 9 mm, and the interval between the ribbons was equal to their thickness and was also 3 mm. The radius of the outer surface of the outer tape was 23.55 mm. The tapes were immersed in a vacuum.

Figure 2 shows a variant of the metacell design, in which the cuts in the tapes are located on the vertical Z-axis. The simulation results of this design (Fig. 3) indicate the existence of many frequency ranges in which the relative magnetic permeability is negative. At the same time, there are also so-called binegative zones, within which not only the magnetic but also the dielectric permittivity becomes negative ($\mathrm{Re}(\varepsilon) < 0$ and $\mathrm{Re}(\mu) < 0$). Since it is these zones that are of the greatest interest, let us analyze the effect of various parameters of the metacell geometry on them. The calculation of ε and μ values will use the special macros that are embedded in HFSS [12].

It should be noted that in the considered version of the outer tape, the depth of the grooves was constant along the entire length. At the same time, the grooves themselves from different ends of the outer tape were arranged in a checkerboard pattern. Next, we study the influence of the variable depth of the grooves, for example, when the cuts of the rings lie in the horizontal plane (Fig. 4), and the grooves on the end surfaces of the outer tape are symmetrical.

Efforts made to vary the design of the metacell made it possible to achieve the appearance of the DNG band in the range of 640–950 MHz (Fig. 5).

A variant of the horizontal arrangement of rings (Fig. 6) was also studied, which is a typical case in the formation of metalenses.

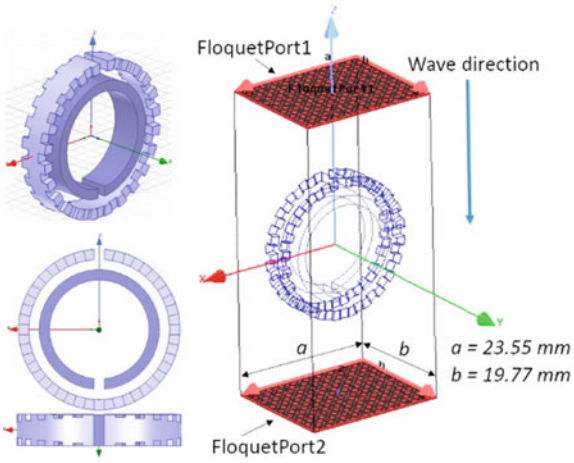

Fig. 2 Appearance of the 3D SRR model from different view angles

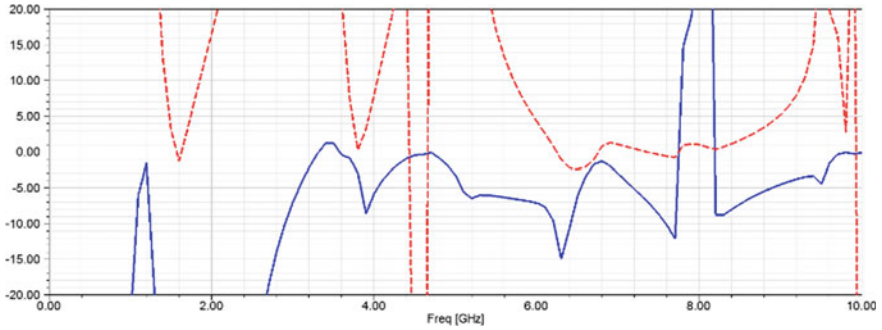

Fig. 3 Evaluation of the characteristics of the SRR model on Fig. 2, solid—Re(ε); dash—Re(μ)

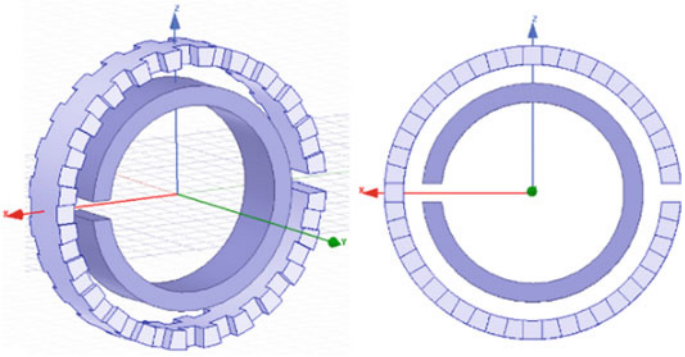

Fig. 4 Vertical orientation option of the SRR model on Fig. 2

At a variable depth of the grooves, the DNG section shifted to the regions of 7.0–7.7 and 7.9–9.25 GHz (Fig. 7), while the zone of negative magnetic permeability values covers a continuous region starting from about 5.3 GHz and beyond 10 GHz. The latter testifies to the prospects of using such structures for constructing magnetic metalenses, for example, for electron microscopes, naturally, provided that the sizes of metarings are scaled in accordance with a given wavelength.

At the end of the first stage of research, a variant of the ring structure with an external tape in the form of a meander was considered (Fig. 8) [15].

For this design, the area of negative permeability of interest is concentrated in the low-frequency range up to about 1.4 GHz (Fig. 9).

In the second stage of research, a transition was made to the combination of split rings and a straight conductor, traditional for metacells, taking into account 3D design. An example of this kind is shown in Fig. 10, while the slot in the outer ring is at the top of the Z-axis, and the center of the cross-section of the conductor is located at a distance of 4 mm from the center of symmetry of the rings. The grooves in the upper band varied in depth according to a sinusoidal law. Such a change in

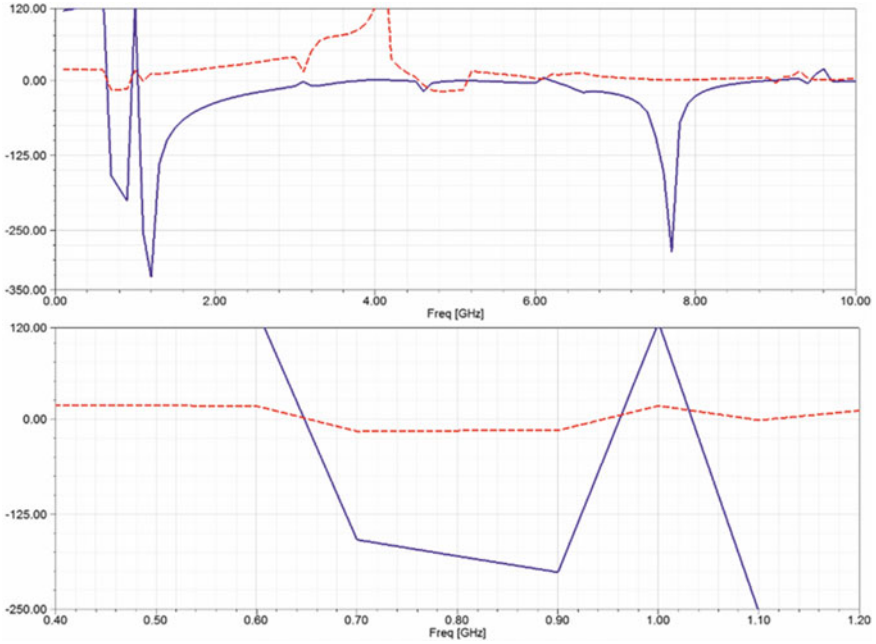

Fig. 5 Emergence of the DNG band in the range of 640–950 MHz, solid—Re(ε); dash—Re(μ)

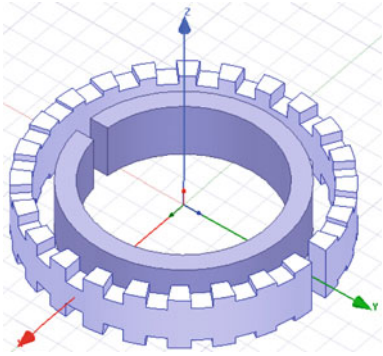

Fig. 6 Metacell with the horizontal orientation

the meander depth is an approximation of the second iteration of the meander-based quasi-fractal.

An important achievement of this design (Fig. 11) was the appearance of a low-frequency range with simultaneously negative values of permittivity and permeability in the region of frequencies from 100 to 336 MHz (100 MHz is the lower limit of calculations).

An important achievement of this design (Fig. 11) was the appearance of a low-frequency range with simultaneously negative values of permittivity and permeability

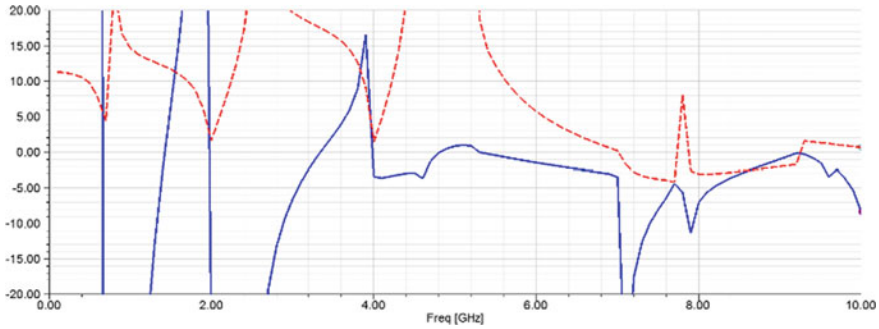

Fig. 7 DNG metacell properties; the solid line is Re(ε); the dashed line—Re(μ)

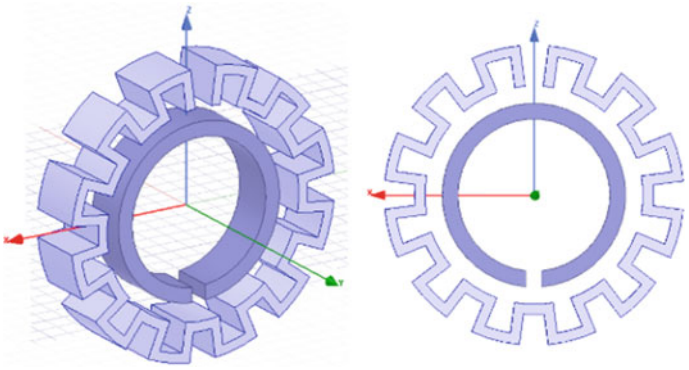

Fig. 8 Quasi-fractal SRR with an outer band in the form of a meander

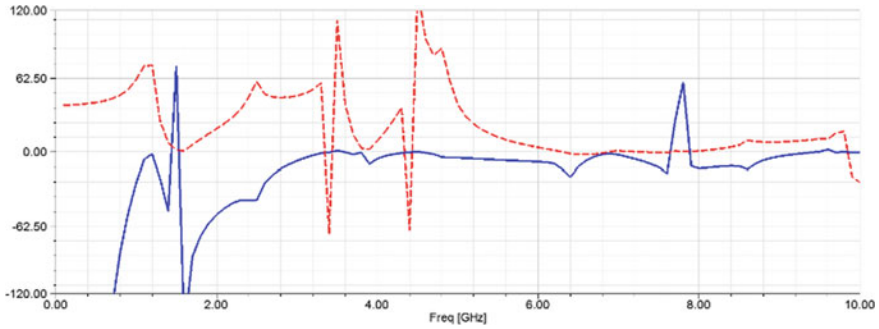

Fig. 9 DNG of the SRR in Fig. 8, solid—Re(ε); dash—Re(μ)

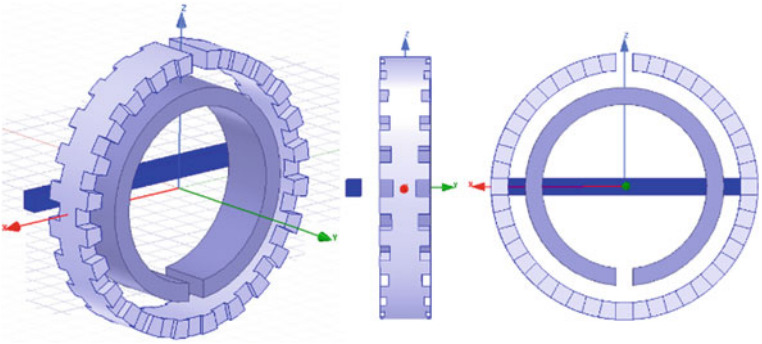

Fig. 10 Appearance of a 3D model of a metacell with a rectangular conductor

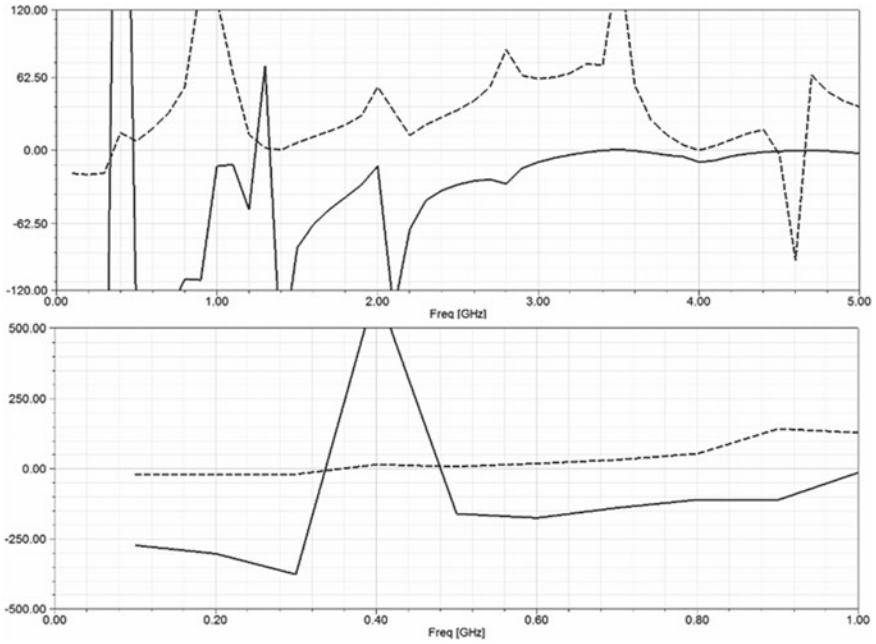

Fig. 11 DNG in the low-frequency region from 100 to 336 MHz, of the metacell in Fig. 10, solid—Re(ε); dash—Re(μ)

in the region of frequencies from 100 to 336 MHz (100 MHz is the lower limit of calculations).

The performed analysis confirmed the insignificance of the influence of the distance of the conductor from the surface of the rings on the width of the DNG range in the low-frequency region. In particular, an increase in this distance from 4 to 10 mm shifted the upper limit of the specified range to 342.6 MHz.

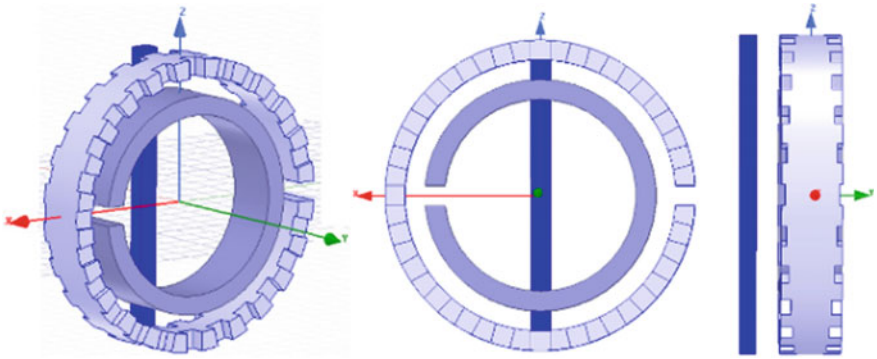

Fig. 12 Metacell vertical orientation option

A more significant result regarding the influence of the length of the low-frequency zone DNG made it possible to obtain an alternative variant of changing the design of the metacell, which consists of the vertical turn of the wire and the location of the cuts of the tapes in the horizontal plane (Fig. 12).

As can be seen from Fig. 13, the transition to a vertical wire extended the upper limit of the DNG zone in the low-frequency region to 647 MHz. At the same time, the second DNG zone was localized in the region of 4.65–5.15 GHz (Fig. 14).

Summarizing the results of the second stage, we can draw intermediate conclusions. In particular, in order for the DNG zone to be in the lower frequency region, it is necessary to place the cut in the outer tape at the top of the *Z*-axis or in the horizontal plane. The location of the cut in the outer ring on the *Z*-axis from below leads to the disappearance of DNG in the low-frequency region.

Since the vertical orientation of the conductor may have certain errors, it is of interest to study the influence of the angles of its deviation from the vertical axis. In particular, the limiting case of conductor deviation from the vertical by 45° was considered (Fig. 15). At the same time, the slots in the tapes were placed on the vertical axis.

The result of such manipulations was the narrowing of the band of the binegative zone to 340 MHz. The lion's share in such a deterioration in the properties of the cell was made not by the deflection of the conductor, but by the turn of the rings to align the slots with the vertical axis. Therefore, we can conclude that in order to maximize the expansion of the lower DNG strip in the case under consideration, it is necessary to place cuts in the ribbons in a horizontal plane. The deviation of the conductor from the vertical at an angle of up to 45° does not affect significantly (Fig. 16).

The next stage of the research consisted of the transition to a conductor located, similarly to [12], perpendicular to the plane of the rings (Fig. 17).

At the same time, the grooves in the uppercut tape at both ends had a variable depth and were located in a synchronous manner; that is, the grooves from opposite ends were opposite each other. An important nuance was also that the sections of the tapes lay in a horizontal plane.

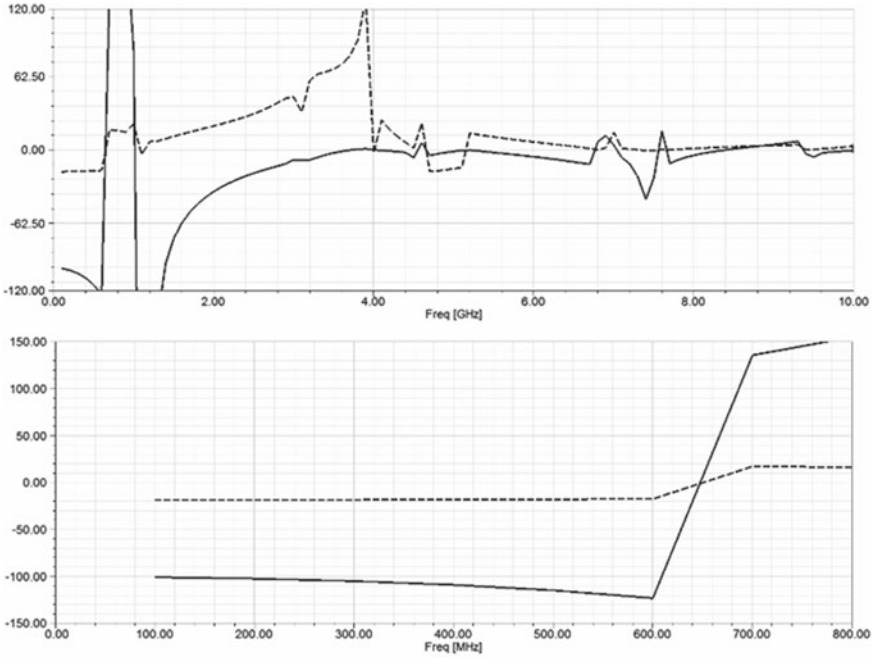

Fig. 13 DNG metacells in Fig. 12 and its band in the lower frequency region (100–647 MHz), solid—Re(ε); dash—Re(μ)

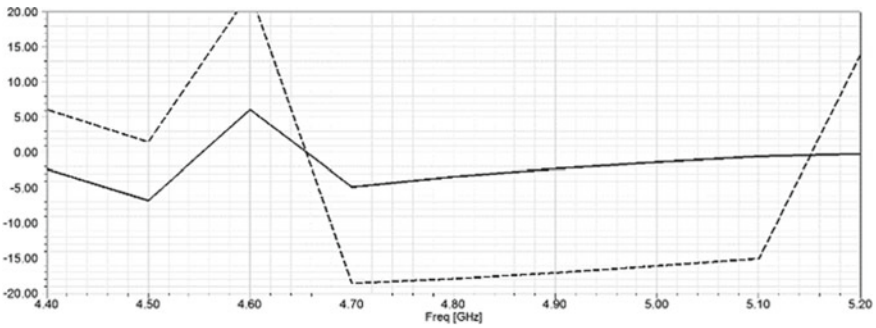

Fig. 14 Localization of DNG in the band of 4.65–5.15 GHz, solid—Re(ε); dash—Re(μ)

As a result of this modification of the metacell design, there was a significant expansion of the DNG bandwidth at lower frequencies, ranging from 25.02 MHz to about 652 MHz (Fig. 18). This corresponds to 185.22% when converted to a relative frequency value according to the fractional bandwidth formula [19–21]:

$$\delta F = \frac{2|f_1 - f_2|}{f_1 + f_2} \tag{1}$$

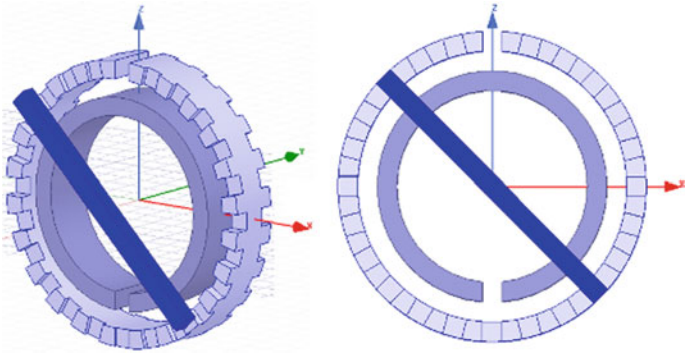

Fig. 15 Metacell with conductor rotated by 45°

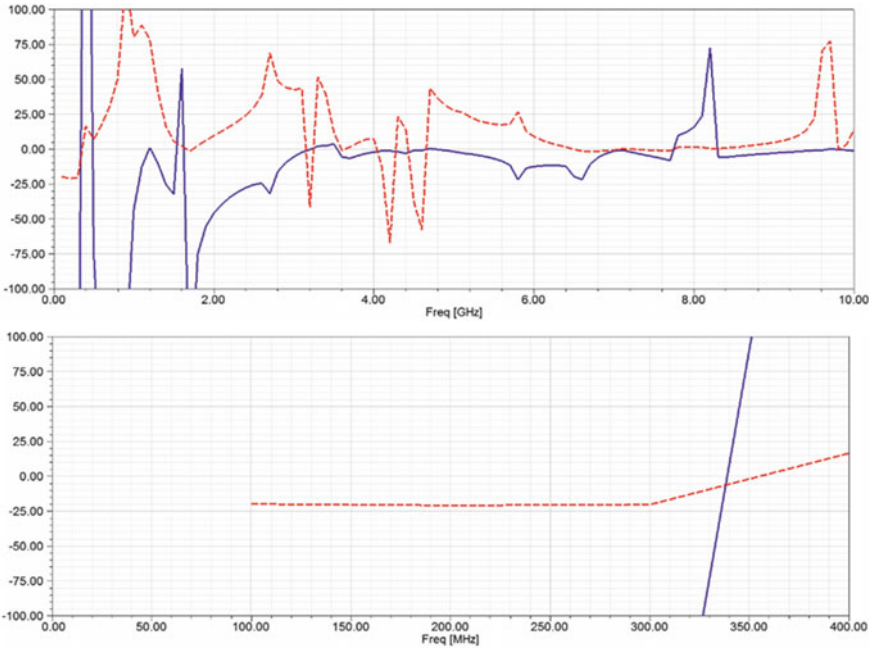

Fig. 16 DNG metacells in Fig. 15 and its low-frequency band, solid—Re(ε); dash—Re(μ)

where f_1 and f_2 are the values of the frequencies at which $\mathrm{Re}(\varepsilon) < 0$ and $\mathrm{Re}(\mu) < 0$.

There are also DNG bands in the ranges from 3.25 to 3.7 GHz and from 4.1 to 5.05 GHz (Fig. 19). Another of these zones is in the range of 8.25–8.75 GHz (Fig. 20).

Thus, the turn of the conductor perpendicular to the plane of the rings (top design), proposed in [12], is an effective solution that led to the expansion of the bandwidths in the corresponding DNG bands.

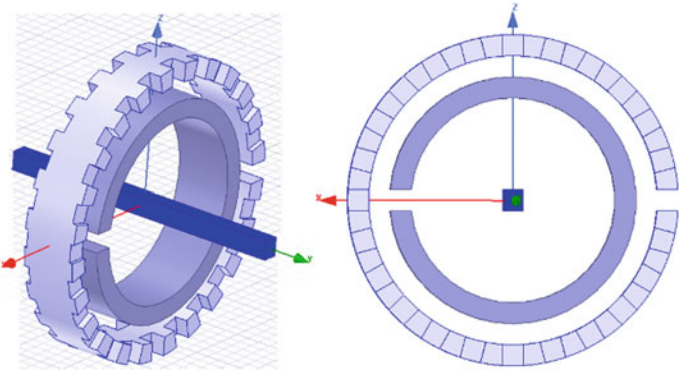

Fig. 17 Modification of a metacell with a rectangular conductor

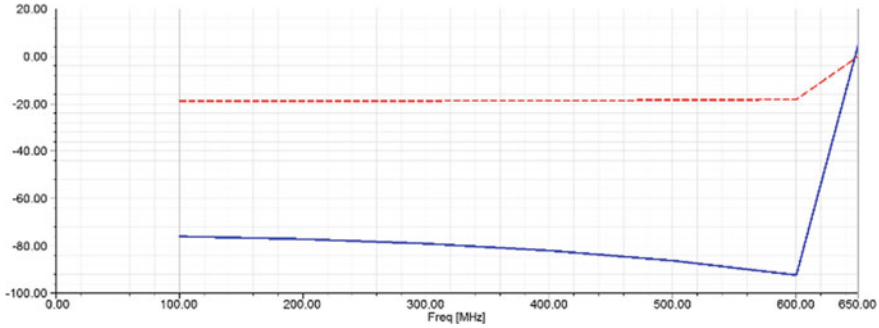

Fig. 18 Lower DNG zone metacell in Fig. 17, solid—Re(ε); dash—Re(μ)

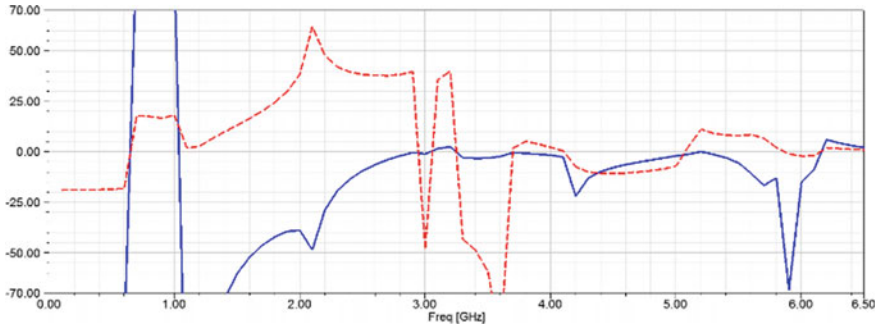

Fig. 19 Central DNG zone metacell in Fig. 17, solid—Re(ε); dash—Re(μ)

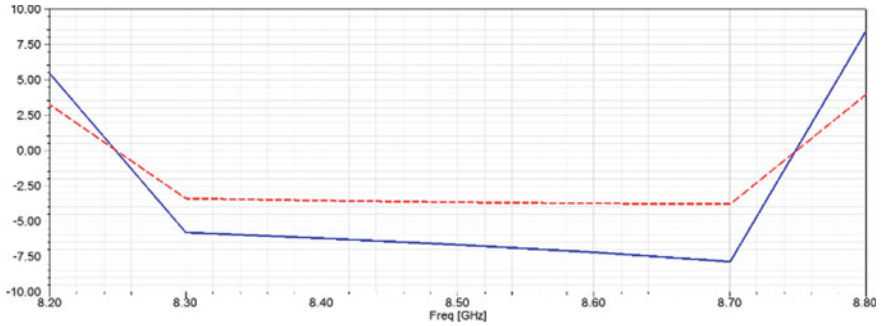

Fig. 20 Upper DNG zone metacell in Fig. 17, solid—Re(ε); dash—Re(μ)

As expected, with a vertical arrangement of the conductor and a horizontal arrangement of the rings (in the X_0Y plane, Fig. 21), similarly to Fig. 6, the DNG band disappears in the low-frequency region (Fig. 22).

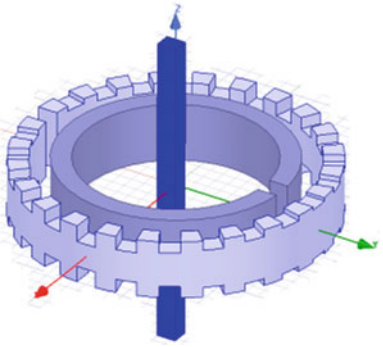

Fig. 21 Horizontal metacell orientation in Fig. 17

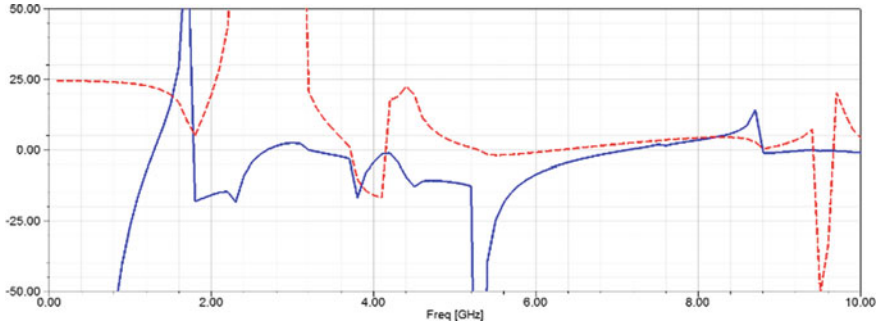

Fig. 22 Evaluation of the characteristics of the metacell model in Fig. 21, solid—Re(ε); dash—Re(μ)

However, in this case, if the conductor is placed horizontally, parallel to the plane of the rings, as shown in Fig. 23, then the specified low-frequency section is restored (Figs. 24 and 25). At the same time, its width becomes relatively smaller (0.1–0.44 GHz, Fig. 25). At the same time, the DNG bandwidth in the region of 7.05–7.75 GHz is 700 MHz (Fig. 26). If, however, the conductor is placed in the intra-annular space (Fig. 27), then regardless of its orientation relative to the cuts in the rings, the low-frequency range of the DNG disappears.

At the final stage of research, attention was paid to variants of the metacell design, with a conductor perpendicular to the plane of the rings and with cuts in the tapes located on the vertical axis (Figs. 28 and 29).

If we set the width of the cut equal to the width of the cross-section of the conductor (2.5 mm), then when the cuts are located on the *Z*-axis, the DNG region in the low-frequency region will disappear (Fig. 30). At the same time, the DNG region is preserved in the region of 4.8–6.35 GHz.

The deviation of the cut in the upper ring from the *Z*-axis in this case leads to the restoration and expansion of the band of the low-frequency section of the DNG as the cuts deviate from the vertical position.

The maximum strip in this design option is achieved when the cuts are located in a horizontal plane (deviation 90° from the *Z*-axis). At the same time, the presence

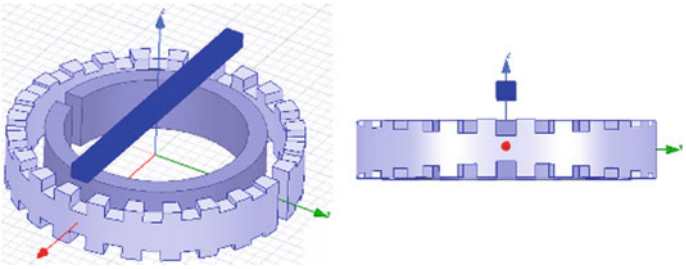

Fig. 23 Horizontal metacell orientation in Fig. 10

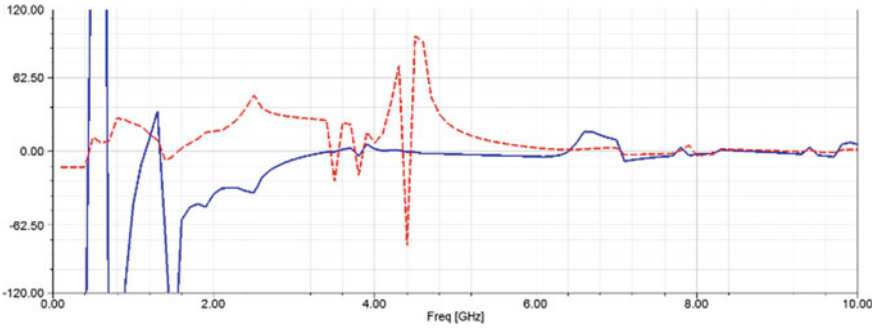

Fig. 24 DNG metacell in Fig. 23, solid—Re(ε); dash—Re(μ)

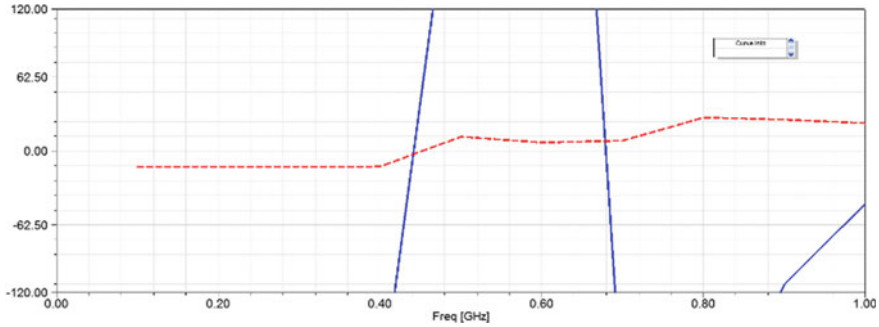

Fig. 25 Lower DNG zone (0.1–0.44 GHz) metacell in Fig. 23, solid—Re(ε); dash—Re(μ)

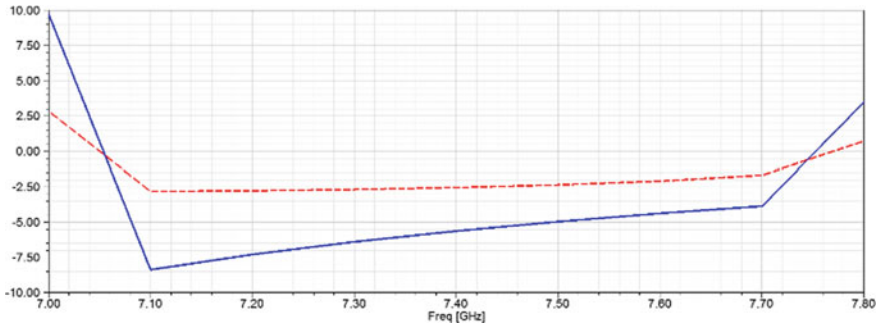

Fig. 26 Upper DNG zone metacell in Fig. 23, solid—Re(ε); dash—Re(μ)

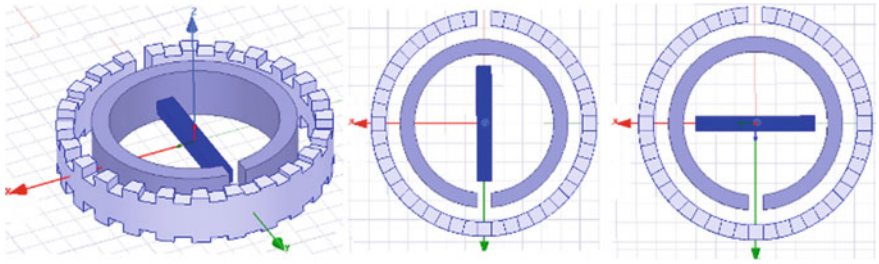

Fig. 27 Placement of the conductor in the annular space of the metacell

of a low-frequency DNG section at 45 and 90° angles of the cut from the *Z*-axis depends on the width of the cut in the ring.

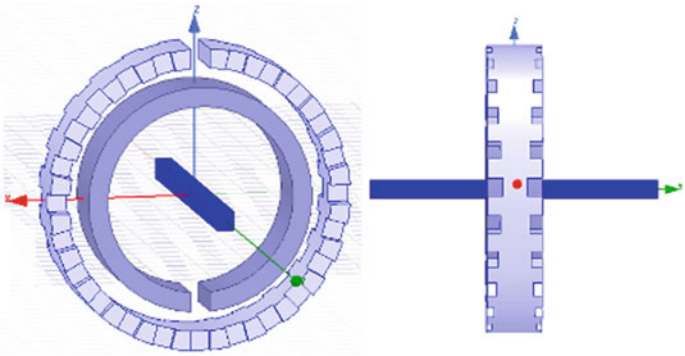

Fig. 28 Metacell layout with ring cuts along the vertical axis

4 Perspectives of Further Research

The presented results were achieved within the framework of the initial stage of generalization of the quasi-fractal approach for SRR synthesis.

Further research should be directed to studying the possibility of expanding the low-frequency zone and obtaining more broadband DNG solutions in other parts of the spectrum. In this regard, the use of sequences of grooves not only in the outer, but also in the inner tape, as well as the search for the optimal combination of their geometric shapes and parameters, deserves attention. In particular, of interest is the use of not only meander lines, but also other geometric figures as the initiator of quasi-fractals, and the study of the influence of dielectric fillers in the intercellular and intra-annular spaces. Further research, of course, will be aimed at preserving the properties of an elementary cell as much as possible in the environment of similar or other elementary cells in the composition of a multi-cell metamaterial. At the same time, not only the influence of the parameters of the relative position, but also the mutual orientation of the metacells in a space will be investigated.

5 Conclusions

The presented results testify to the efficiency of the quasi-fractal approach to the synthesis of metamaterial cells. Among the many variants of the studied SRR, the best solution in terms of the width of the frequency range, in which the condition of negative dielectric permittivity and magnetic permeability is observed, is the use of a conductor oriented perpendicular to the plane of the rings. In this case, the grooves on both ends of the outer tape had a variable depth and were arranged in a synchronous manner. An important nuance is also that the cuts of the tapes lie in a horizontal plane. The indicator of the relative frequency band of the DNG zone achieved in this case was 185.22%. In this sense, the use of a two-ribbon structure as the basis of

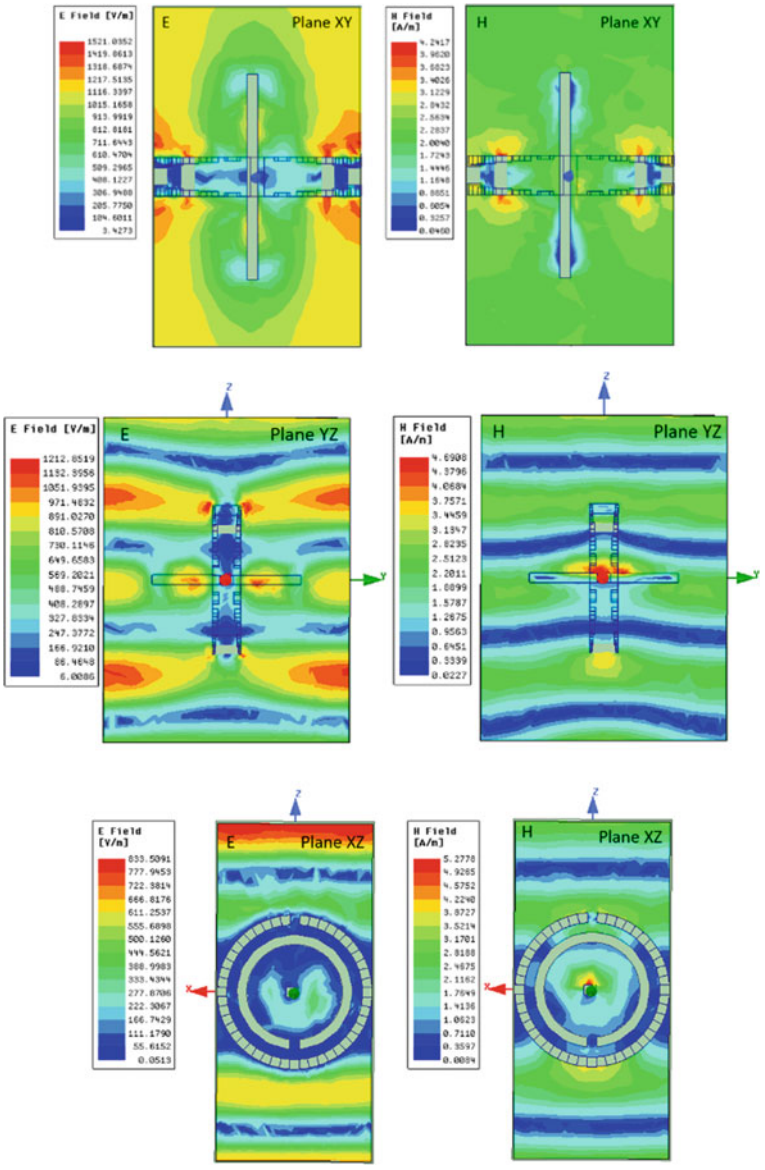

Fig. 29 Fields E and H of the metacell on Fig. 28

a metamaterial cell makes it possible to obtain a wider relative frequency band in comparison with the options for using them as an antenna (in [15], the same indicator did not exceed 132%).

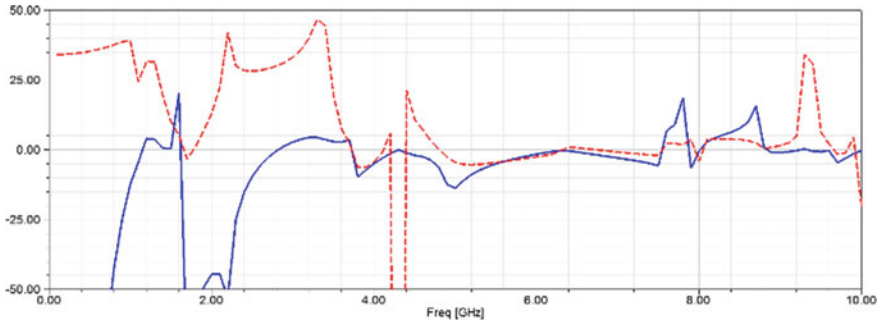

Fig. 30 DNG metacell in Fig. 28, solid—Re(ε); dash—Re(μ)

References

1. Vishnevsky VM, Liachov AI, Portnoj SL et al (2005) Shirokopolosnye besprovodnye seti peredachi informacii [Broadband wireless communication networks]. Technosphera, Moscow, pp 524–526 (in Russian)
2. Slyusar V (2007) 60 years of electrically small antennas theory. In: IEEE 2007 6th international conference on antenna theory and techniques, Sevastopol, pp 116–118. http://doi.org/10.1109/ICATT.2007.4425129
3. Veselago V (1968) The electrodynamics of substances with simultaneously negative values of ε and μ. Sov Phys Uspekhi 10:509–514. https://doi.org/10.1070/PU1968v010n04ABEH003699
4. Veselago V, Braginsky L, Shklover V, Hafner C (2006) Negative refractive index materials. J Comput Theor Nanosci 3(2):189–218. https://doi.org/10.1166/jctn.2006.3000
5. Slyusar V (2009) Metamaterials on antenna solutions. In: IEEE 2009 7th international conference on antenna theory and techniques (ICATT'09), Lviv, pp 19–24
6. Wu M-F et al (2005) Miniaturization of a patch antenna with dispersive double negative medium substrates. In: IEEE 2005 Asia-Pacific conference on microwave proceedings (APMC 2005), China. https://ieeexplore.ieee.org/document/1606177/authors#authors. Last accessed 2022/09/21
7. Chevalier CT, Wilson JD (2004) Frequency bandwidth optimization of left-handed metamaterial. In: NASA/TM–2004-213403. https://ntrs.nasa.gov/archive/nasa/casi.ntrs.nasa.gov/20050019217.pdf. Last accessed 2022/09/21
8. Jaksic Z, Maksimovic M, Dalarsson N (2006) Negative refractive index metamaterials: principles and applications. Microwave Rev 6:36–49
9. Chen C, Hsiao C, Sun S et al (2012) Fabrication of three dimensional split ring resonators by stress-driven assembly method. Opt Express 20(9):9415–9420. https://doi.org/10.1364/OE.20.009415
10. Salim A, Ghosh S, Lim S (2018) Low-cost and lightweight 3D-printed split-ring resonator for chemical sensing applications. Sensors (Basel) 18(9):3049. https://doi.org/10.3390/s18093049
11. Vallecchi A, Shamonina E, Stevens C (2019) Analytical model of the fundamental mode of 3D square split ring resonators. J Appl Phys 125:014901. https://doi.org/10.1063/1.5053482
12. Sliusar I, Slyusar V, Utkin Y, Kopishynska O (2020) Parametric synthesis of 3D structure of SRR element of the metamaterial. In: 2020 IEEE 7th international scientific and practical conference "Problems of infocommunications. science and technology" (PICS&T'2020), Kharkiv, p 6. http://doi.org/10.1109/PICST51311.2020.9468067
13. Matveev E, Potapov A (2009) Fractal antennas for the new class of radio systems: Keily tree and circular monopole. In: International radar symposium (IRS-2009), Hamburg, pp 465–468

14. Mandelbrot B (1977) Fractals: form, chance and dimension. Freeman, San-Francisco, 365 p
15. Sliusar I, Slyusar V, Voloshko S, Zinchenko A, Degtyareva L (2019) Synthesis of quasi-fractal ring antennas. In: IEEE 2019 6th international scientific practical conference on problems of infocommunications, science and technology (PIC S&T), Kyiv, pp 741–744. http://doi.org/10.1109/PICST47496.2019.9061286
16. Sliusar I, Slyusar V, Voloshko S, Zinchenko A, Utkin Y (2020) Synthesis of a broadband ring antenna of a two-tape design. In: IEEE 12th international conference on antenna theory and techniques (ICATT-2020), Kharkiv, pp 161–165. http://doi.org/10.1109/UkrMW49653.2020.9252793
17. ANSYS HFSS, http://www.ansys.com/Products/Simulation+Technology/Electronics/Signal+Integrity/ANSYS+HFSS. Last accessed 2022/09/21
18. Bankov SE, Kurushin AA (2009) Calculation of antennas and microwave structures using HFSS Ansoft [Raschet antenn i SVCH struktur s pomoshchyu HFSS Ansoft]. ZAO NPP "Rodnik", Moscow, pp 207, 208 (in Russian)
19. Assessment of Ultra-Wideband (UWB) Technology. OSD/DARPA ultra-wideband radar review panel. Battelle Tactical Technology Center, Contract No. DAAH01-88-C-0131, ARPA Order 6049, July 13, 1990
20. Sliusar I, Slyusar V, Voloshko S, Degtyareva L (2019) Antenna synthesis based on fractal approach and DRA technologies. In: IEEE 2th Ukraine conference on electrical and computer engineering (UKRCON-2019), Lviv, pp 29–34. http://doi.org/10.1109/UKRCON.2019.8879953
21. Sliusar I, Slyusar V, Voloshko S, Smolyar V (2018) Synthesis of quasi-fractal hemispherical dielectric resonator antennas. In: IEEE 2018 5th international scientific-practical conference problems of infocommunications, science and technology (PIC S&T), Kharkov, pp 313–316. http://doi.org/10.1109/INFOCOMMST.2018.8632087